Translation of Solar Cell Performance for Irradiance and Temperature From a Single *I-V* Curve Without Advance Information of Translation Parameters

Yoshihiro Hishikawa, Takakazu Takenouchi, Michiya Higa, Kengo Yamagoe, Hironori Ohshima, and Masahiro Yoshita

***Abstract*—A practical and accurate procedure for translating the current–voltage (*I–V*) curves of photovoltaic devices for irradiance and temperature is proposed. The procedure requires only a single experimental *I–V* curve with no advance information of the translation parameters when the devices follow the single-diode model. The parameters used in the translation, such as the series resistance R_s and diode ideality factor n, are extracted from the experimental *I–V* curve. A voltage-dependent temperature coefficient of the *I–V* curve, which was recently proposed by the authors, is used for accurate temperature translation. The procedure is shown to be applicable to many commercial crystalline silicon PV modules in wide irradiance and temperature ranges of 0.15–1.1 kW/m^2 and 10–65 °C, respectively, with typical accuracy within ±1%–2%.**

***Index Terms*—Crystalline silicon, *I–V* curve, resistance, p-n junction diode, temperature coefficient, translation.**

TABLE I
EXPERIMENTAL PERFORMANCE PARAMETERS OF THE CRYSTALLINE SILICON PV MODULES USED IN THE PRESENT STUDY, WHICH WERE MEASURED INDOORS UNDER STC

Sample (No. cells)	I_{SC} (A) TC_{rel} (%/K)	V_{OC} (V) TC_{rel} (%/K)	P_{MAX} (W)	FF (%)	Type
N15A01 (40)	9.19 0.047	25.25 -0.32	178.9	77.1	PV-MA1820LW-1 (Mitsubishi, mono)
N15B05 (48)	9.06 0.046	30.18 -0.31	206.5	75.5	KJ210P-3DD4CG (Kyocera, multi)
N16C03 (72)	6.32 0.037	48.3 -0.28	240.4	78.7	SPR-250NE-WHT-J (Sunpower, mono)

The numbers of series-connected cells in the modules are also shown. The values of the relative temperature coefficient TC_{rel} of I_{sc} and V_{oc} under STC are also shown for reference, although they were not used in the present study.

I. INTRODUCTION

TRANSLATION of the current–voltage (*I–V*) curves is necessary in various kinds of characterization of photovoltaic (PV) devices. It is especially important for outdoor performance measurements, where the curves measured under various irradiance and temperature conditions are translated to STC (standard test conditions—irradiance of 1 kW/m^2, spectrum of AM1.5G, and module temperature of 25 °C) [1]. Conventional translation procedures, such as [2, Procedures 1 and 2], are based on advance information of translation parameters such as the series resistance (R_s), temperature coefficient of open circuit voltage V_{oc}, (β), curve correction factor (κ), etc. Therefore, accurate translation was impossible without those parameters. The situation was problematic for many outdoor measurements of PV modules for on-site inspection, since those parameters are usually not fully described in their nameplates. Although the linear interpolation method [3], which is also described as [2, Procedure 3], uses no such translation parameters, it requires at least two, and preferably three to four, reference *I–V* curves which cover the irradiance and temperature ranges of interest. Those were not easily available in outdoor measurements in a short period of time.

The present study proposes a new translation procedure, which is capable of translation for irradiance and temperature from a single experimental *I–V* curve, without advance information of the translation parameters. It is applicable to PV devices which follow the single-diode model, and the outline was briefly presented in [4]. The present study discusses its background, basic applicability and detailed formulas, and verifies the procedure by many indoor and outdoor experimental results.

II. EXPERIMENT

A. Indoor Measurements

The *I–V* curves of commercial crystalline silicon PV modules as shown in Table I, which will be hereafter denoted as modules under test (MUTs), were measured at irradiances of about 0.15 and 1 kW/m^2, and module temperatures of about 10, 25, 45, and 65 °C by using a large area multijunction module solar simulator LAMS at AIST. Specific stabilization procedure was not applied to the MUTs before the measurements. Typical measurement time for each *I–V* curve was 0.1–0.3 s. A thermostatic chamber was used for controlling the module temperature. Other details of the indoor measurements are described in [5]. The indoor STC *I–V* measurements of the MUTs were carried out before

Manuscript received January 23, 2019; revised April 5, 2019 and May 18, 2019; accepted June 9, 2019. This work was supported by the New Energy and Industrial Technology Development Organization (NEDO), Ministry of Economy, Trade and Industry (METI), Japan. *(Corresponding author: Yoshihiro Hishikawa.)*

The authors are with the Research Center for Photovoltaics, National Institute of Advanced Industrial Science and Technology, Tsukuba 305-8568, Japan (e-mail: y-hishikawa@aist.go.jp; t-takenouchi@aist.go.jp; m.higa@aist.go.jp; k-yamagoe@aist.go.jp; hironori-ohshima@aist.go.jp; m-yoshita@aist.go.jp).

Color versions of one or more of the figures in this paper are available online at http://ieeexplore.ieee.org.

Digital Object Identifier 10.1109/JPHOTOV.2019.2924388

and after the outdoor measurements, which showed agreement in the short circuit current $I_{\rm sc}$, $V_{\rm oc}$, and maximum output power $P_{\rm max}$ within $\pm 0.4\%$.

B. Outdoor Measurements

The *I–V* curves of the MUTs in Table I were measured using an ADC 4601 *I–V* meter at a sweep time of 0.2 s and an interval of 5 s throughout the daytime. The MUTs were mounted on a fixed open rack facing 25° southwest with a 15° tilt angle, on the rooftop of a building at AIST Tsukuba Center, Japan. The solar irradiance was measured using a PV module irradiance sensor (PVMS), which comprises of an active 5-in c-Si cell and eight dummy cells around it. The PVMS was located within 1 m to the MUT on the same rack. Its azimuth and tilt angle were the same as those of the MUTs within 0.5°. The PVMS enables accurate irradiance measurements for PV performance characterization, thanks to its very similar response time, spectral responsivity, and angular response to the MUTs [6], [7]. The temperature of each MUT was monitored using resistive temperature sensors (Pt100) attached to the backsheet. Other details of the outdoor measurements are described in [8].

III. Results and Discussion

The *I–V* curve translation procedure of the present study first extracts two diode parameters (R_s and diode ideality factor n) from a single experimental curve. Then, the curve is translated for irradiance by using the R_s. Following that, it is translated for temperature by using the voltage-dependent temperature coefficient [5]. Although n is not necessarily used in the translation, it may be used for extending the curve, when the voltage range of the experimental curve is not enough.

A. Determination of R_s and n

The *I–V* curve of a PV module is often expressed by the single-diode model as

$$I = I_L - I_0 \left[\exp\left\{ \frac{q\,(V + R_s I)}{N_c n k T} \right\} - 1 \right] - \frac{V + R_s I}{R_s}. \quad (1)$$

When the effect of R_{sh} is negligible, i.e., when the R_{sh} is very large, or the shunt conductance is close to zero, it can be approximated by

$$I = I_{\rm SC} - I_0 \exp\left\{ \frac{q\,(V + R_s I)}{N_c n k T} \right\}. \quad (2)$$

The effect of R_{sh} will be mentioned later. Here, q, k, T, I_L, I_0, and N_c are the electron charge, Boltzmann's constant, device temperature, photocurrent, diode saturation current, and number of series-connected cells, respectively.

There have been many studies and reviews on methods for estimating R_s from experiments [9]–[21]. Some of them use two or more experimental *I–V* curves at various irradiance levels [12]–[14]. However, the present study uses a single *I–V* curve, in order to enable translation even when such systematic experimental *I–V* curves are not available. Warashina and Ushirokawa [15] presented a method to determine R_s and n by using the linear relationship between dV/dI and $1/(I_{\rm sc} - I)$, which is derived by differentiating (2)

$$-\frac{\partial V}{\partial I} = \frac{N_c n k T}{q} \frac{1}{I_{\rm sc} - I} + R_s. \quad (3)$$

Similar approaches which use the *dI/dV* of the dark *I–V* curves of Schottky diodes are also proposed in [16]. Although (3) offers a simple method for extracting the parameters, its differential form tends to introduce estimation errors, since experimental values of *V* and *I* are discrete. Therefore, the present study uses the following difference formula:

$$-\frac{V_a - V_b}{I_a - I_b} = -\frac{N_c n k T}{q} \frac{\ln(I_{\rm sc} - I_a) - \ln(I_{\rm sc} - I_b)}{I_a - I_b} + R_s. \quad (4)$$

Here, (V_a, I_a) and (V_b, I_b) are the voltages and currents of two data points A and B, respectively, on an *I–V* curve, as shown in Fig. 1. Equation (4) is also derived from (2). Its equivalent form was presented by El-Adawi and Al-Nuaim [17], as well as, mentioned in [11]. The present study first systematically employs the equation for extracting R_s from the *I–V* curves of different kinds of MUTs under various conditions, and uses R_s for translating the curves to STC. The translated curves are compared with the experiments for verifying the practical validity of the procedure.

An example of parameter extraction based on (4) is illustrated in Fig. 2(a), wherein $-(V_a - V_b)/(I_a - I_b)$ is plotted versus $-\{\ln(I_{\rm sc} - I_a) - \ln(I_{\rm sc} - I_b)\}/(I_a - I_b)$. The points A and B are chosen to be next to each other and scanned through the *I–V* curve of Fig. 1. The *y*-intercept of the plot shows R_s, and its slope shows $N_c n k T/q$. The plot forms nearly a straight line with a coefficient of determination (R^2) of 0.9961, which indicates that the *I–V* curve nearly follows the single-diode model of (2). Slight noise in the plot, primarily because of the small fluctuation of the solar simulator light, is seen in the figure. The noise can be reduced by utilizing the fact that (4) is valid for any combination of $(V_a,\ I_a)$ and $(V_b,\ I_b)$ on the *I–V* curve. For example, Fig. 2(b)

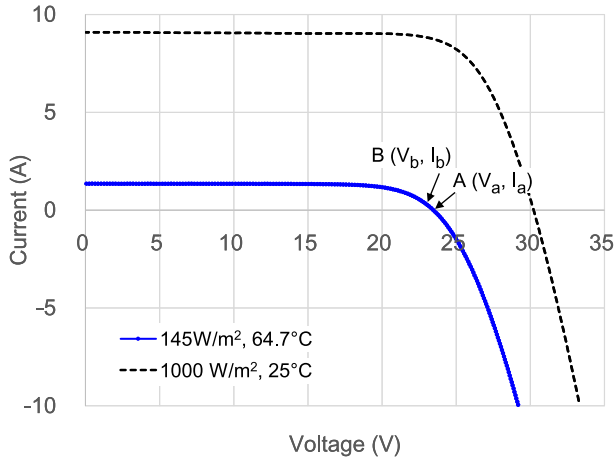

Fig. 1. Indoor *I–V* curve of N15B05 under an irradiance of about 145 W/m^2 and module temperature of 64.7 °C is shown by blue symbols with line. The curve under 1 kW/m^2 and 25 °C is shown by a black dashed line. Examples of data points A (V_a, I_a) and B (V_b, I_b) for extracting R_s by (4) are also pointed by arrows.

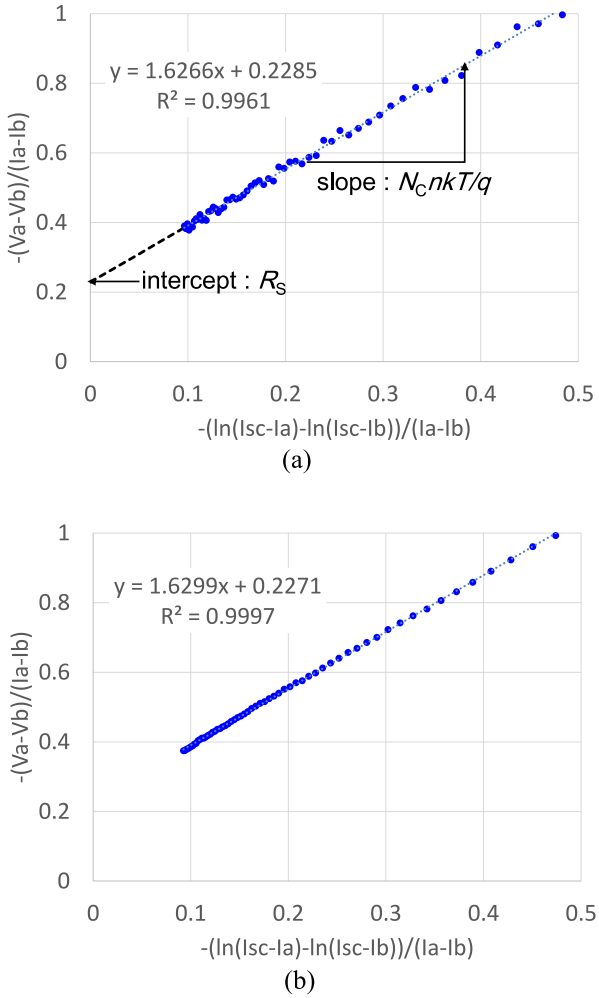

Fig. 2. Examples for the determination of R_s and n from an indoor *I–V* curve. Values of $-(V_a–V_b)/(I_a–I_b)$ in Fig. 1 is plotted versus $-\{\ln(I_{sc}–I_a) - \ln(I_{sc}–I_b)\}/(Ia–I_b)$. (a) Data points A and B are chosen to be next to each other. (b) A and B are chosen so that five data are left between them.

shows a plot based on the identical data set as in Fig. 2(a), where the points A and B are chosen so that five data are left between them. The plot in Fig. 2(b) has smaller fluctuation than that in Fig. 2(a), which is also reflected in the R^2 being very close to unity (i.e., 0.9997 as shown in the figure), allowing more accurate estimation of R_s and n. The reduction of noise is simply because the values in (4), such as $V_a - V_b$ and $I_a - I_b$, become larger by leaving some data points between A and B; hence, the relative impact of the random noise becomes smaller. It is noted that there have also been other methods for extracting R_s and n from a single *I–V* curve [18]–[21], many of which use the performance parameters, such as I_{sc}, V_{oc}, P_{max}, etc., instead of the *I–V* curve. The advantage of the present method is that many data points in the curve can be utilized so that the random noise is averaged out in the plot, as shown in Fig. 2(b). Another advantage is that the straightness of the plot or the R^2 is a good criterion of whether the *I–V* curve follows the single-diode model, since (4) is equivalent to (2).

Data points in the highest voltage region of the *I–V* curve should be used for the plot, since its low-voltage region usually deviates from a straight line, influenced by the shunt resistance R_{sh}. Inequality of the component cells' individual I_{sc} within the MUT also possibly affects the linearity of the plot. These factors are not considered in the present study, since good translation results are usually obtained without considering them, as demonstrated in the later sections. Although an iterative method to take into account the R_{sh} based on a single *I–V* curve was proposed in [22], explicit consideration of both R_{sh} and the inequality of the individual I_{sc} will make the equation more complicated, which is an issue for future study. It is noted that the error in R_s determination possibly becomes more sensitive to the experimental noise or error in the *I–V* curve when the number of data points in the *I–V* curve becomes fewer, because the number of data points in the linear part of the plot becomes fewer. Clear criteria of R^2 and the number of points for the plot are not defined in the present study, since they are influenced by many factors such as experimental conditions, experimental errors, and specific features of the device. A practical example would be $R_2 > 0.995$ for more than ten points in the plot. A fewer number of points may also yield a reasonable value of R_s, if R^2 is closer to unity.

B. Translation of I–V Curves

Based on the extracted R_s, the *I–V* curve is first translated for irradiance by using

$$I' = I_1 + I_{sc1} \cdot \left(\frac{G_2}{G_1} - 1\right) \tag{5}$$

$$V_1' = V_1 - R_s \cdot (I'_1 - I_1) \tag{6}$$

which is equivalent to the irradiance correction in [2, Procedure 1]. Then, the curve is corrected for temperature by using

$$I_2 = I_1' + \alpha_{rel} I'_{sc1} (T_2 - T_1) \tag{7}$$

$$V_2 = V_1' + \frac{T_2 - T_1}{T_1} \cdot \left(V'_1 - \frac{N_c n E_g}{q}\right). \tag{8}$$

Here

V_1, I_1: (initial condition, blue solid circles in Fig. 3) voltage and current of data on an *I–V* curve under irradiance G_1 and module temperature T_1;
I_{SC1}: I_{sc} under irradiance G_1 and module temperature T_1;
V_1', I_1': (intermediate condition, blue x symbols in Fig. 3) those under irradiance G_2 and module temperature T_1;
I'_{SC1}: I_{sc} under irradiance G_2 and module temperature T_1;
V_2, I_2: (final condition, red open circles in Fig. 3) those under irradiance G_2 and module temperature T_2;
E_g: bandgap of the photovoltaic material;
α_{rel}: temperature coefficient of I_{sc}.

The present study uses the voltage-dependent temperature coefficient, which is expressed by (8) [5]. Although the value of nE_g/q is basically device dependent, a value of $nE_g/q = 1.232$ V is a good approximation for various commercial crystalline silicon devices [5]. It has also been recently reported that

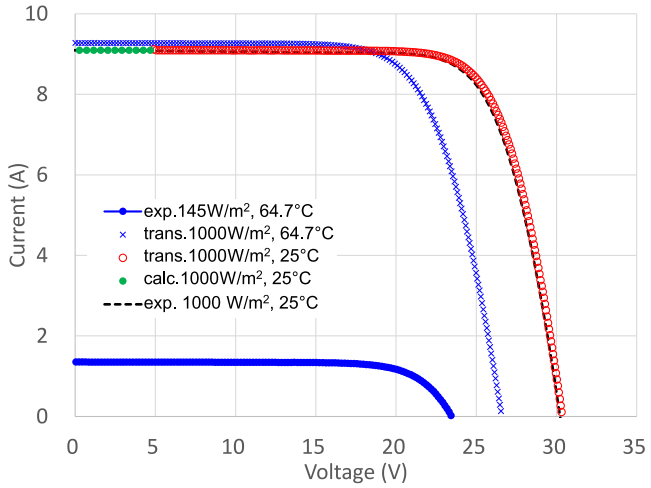

Fig. 3. Typical translation results. Blue circles with line are the same experimental *I–V* curve as shown in Fig. 1, whose negative current region is not shown. Blue x symbols show the data translated to 1 kW/m^2 by (5) and (6). Red open circles are the data subsequently translated to 25 °C by (7) and (8). Green solid circles are data extended to lower voltage by (2). The black dashed line shows the experimental curve under STC.

$\alpha_{\rm rel}$ ranges around 0.03–0.06%/K for crystalline silicon modules depending on their spectral responsivity [23], and may be approximated as 0.05%/K without large discrepancies of translated results [5]. Equations (5)–(8) can be combined into

$$I_2 = I_1 + I_{\rm sc1}.\left[\frac{G_2}{G_1}\left\{1+\alpha_{\rm rel}\left(T_2-T_1\right)\right\}-1\right] \tag{9}$$

$$V_2 = V_1 - R_s I_{\rm sc1}\cdot\left(\frac{G_2}{G_1}-1\right)+\frac{T_2-T_1}{T_1}\cdot \left\{V_1 - R_s I_{\rm sc1}\cdot\left(\frac{G_2}{G_1}-1\right)-\frac{N_c n E_g}{q}\right\} \tag{10}$$

if $I_{\rm sc}$ is linear with irradiance [24] (i.e., $I'_{\rm SC1} = I_{\rm SC1}\cdot G_2/G_1$), which is a good approximation for many PV devices. They enable direct translation from (V_1, I_1) to (V_2, I_2).

When necessary, the *I–V* curves can also be extended beyond the measured voltage range based on (2). For example, the translated *I–V* curve (red open symbols in Fig. 3) does not have data at voltages smaller than 5 V. Data in the voltage range can be calculated by using the extracted R_s and $N_c nkT/q$ based on (2), as shown by the green solid circles in Fig. 3. The I_0 used for the calculation can be determined by

$$I_0 = (I_{\rm SC} - I)\cdot\exp\left\{-\frac{q\left(V+R_s I\right)}{N_c nkT}\right\} \tag{11}$$

where V and I are the voltage and current of a point on the *I–V* curve. The values at higher voltage usually result in smoother connection of the extended curve with experimental data. It is noted that R_s influences the translation through the term $R_s\cdot(I'_{\rm SC1} - -I_{\rm SC1})$ in (6). For example, the small difference of 1.4 mΩ in R_s in Fig. 2, i.e., 0.2285 Ω in Fig. 2(a) and 0.2271 Ω in Fig. 2(b), depending on the choice of data points, corresponds to the voltage difference of about 10 mV when $I'_{\rm SC1} - I_{\rm SC1}$ is 7 A. It is negligibly small, being about 0.03% of the $V_{\rm oc}$ of the MUT under STC.

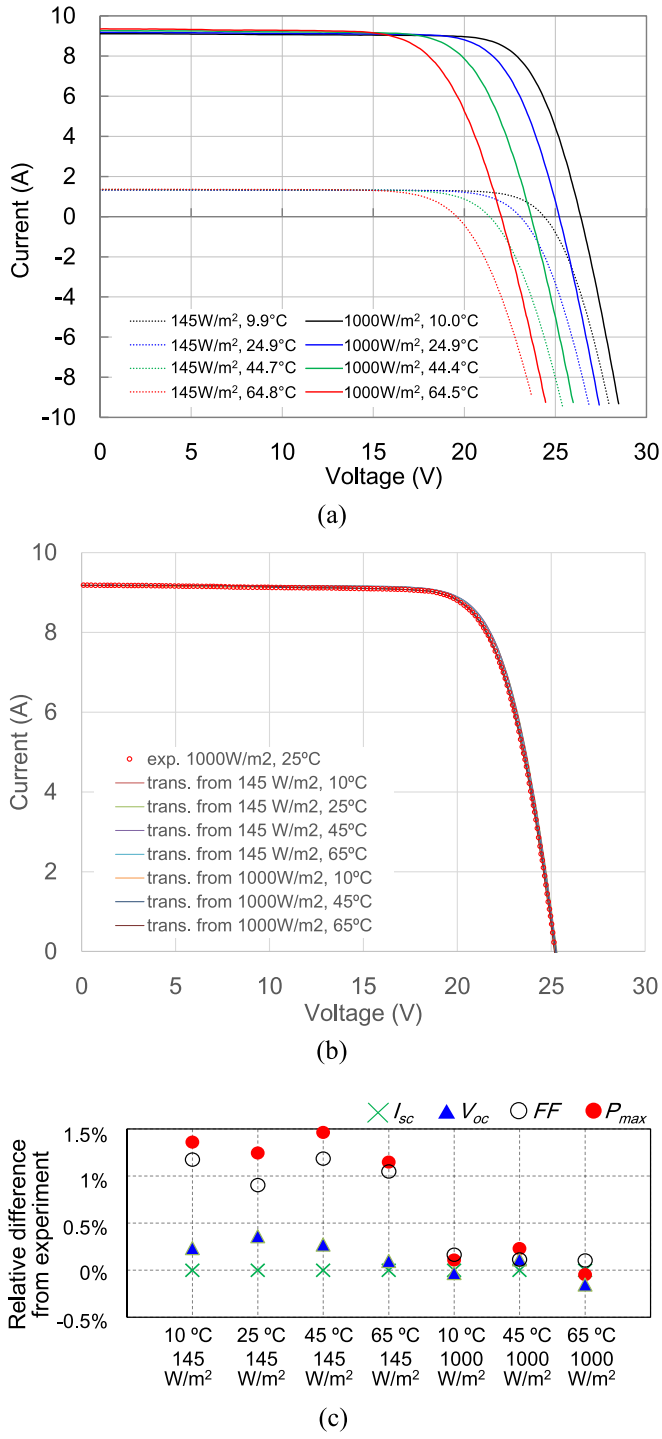

Fig. 4. (a) Indoor *I–V* curves of N15A01. The measured irradiance and module temperature are indicated in the legend. (b) *I–V* curves translated to STC from the curves in (a). (c) Relative difference of the parameters of translated and experimental STC *I–V* curves as shown in (b).

C. Verification by Indoor Measurements

I–V curves measured indoors as shown in Fig. 4(a) were translated to those under 1 kW/m^2 and 25 °C by the procedure described above. The results are shown in Fig. 4(b) by lines. The $V_{\rm oc}$, FF, and $P_{\rm max}$ of all the translated curves agreed within −0.5% to +1.5% of the experimental values as illustrated in

Fig. 4(c), which demonstrates the excellent translation accuracy. $\alpha_{\rm rel}$ was assumed to be 0.05%/K, and G_2 was chosen so that the experimental $I_{\rm sc}$ is reproduced, since the purpose here is to verify the accuracy of the translation procedure, for which the detailed value of $I_{\rm sc}$ is not critical. It should be noted that the effect of potential nonlinearity of the MUT and PVMS is not reflected in Fig. 4(b) and (c), because of the choice of G_2.

D. Verification by Outdoor Measurements

Outdoor *I–V* curves were also investigated for verifying the translation procedure. $\alpha_{\rm rel}$ was assumed to be 0.05%/K, and G_2 was chosen so that the experimental $I_{\rm sc}$ is reproduced. It is noted that the outdoor *I–V* measurements in the present study used the PVMS as an irradiance sensor, thereby improving the measurement reproducibility to a level of $\pm 0.5\%$ [6]–[8]. However, the reproducibility is still slightly inferior to the indoor measurements, mainly because of the instability and nonuniformity of irradiance and temperature. The negative current or forward current region of the outdoor *I–V* curves was not measured in the present study, because of the specification of the *I–V* tester. It also tends to make the error in R_s estimation larger, since the straight region of the plot in Fig. 2 becomes shorter. The experimental curves shown in Fig. 5(a) cross at various voltages, since they were measured under various irradiance and temperature, as indicated in the figure legend. Nevertheless, all the curves corrected to STC shown in Fig. 5(b) agree within -1.5% to $+1\%$ for $V_{\rm oc}$, FF, and $P_{\rm max}$ as illustrated in Fig. 5(c), which demonstrates the capability of accurate translation of outdoor *I–V* curves in the present study.

Further verification of the translation procedure was carried out by using many outdoor *I–V* curves of the MUTs. Thousands of *I–V* curves measured on partly sunny or cloudy days were investigated, in order to verify the applicability of the procedure under unstable solar irradiance. It has been recently shown that the nonuniformity of irradiance between the MUT and PVMS, as well as, that within the MUT is an important factor for achieving reproducible outdoor *I–V* measurements under unstable outdoor conditions [6]. Therefore, the *I–V* curves were omitted in the present study, if the variation of irradiance during 5 s was larger than 0.3%, which can effectively filter out the data measured under nonuniform irradiance, because of the partial shading of sunlight caused by moving clouds [25], [26]. Also, the *I–V* curves which yield a straight line with $R^2 > 0.9998$ and more than seven points in the plot shown in Fig. 2 were used, for ensuring proper extraction of R_s and n. Although these conditions filtered out some of the data, usually more than 1000 *I–V* curves were translated to STC for each day except for rainy days. $\alpha_{\rm rel}$ was assumed to be 0.05%/K for all the MUTs. Typical results for N15A01 are summarized in Fig. 6(a), where the parameters of the outdoor *I–V* curves, which are translated to STC by the procedure described above, are compared with the indoor STC values. The $I_{\rm sc}$, $V_{\rm oc}$, FF, and $P_{\rm max}$ results are shown by green, blue, black, and red symbols, respectively. The irradiance and module temperature of the day are also shown by the inset. Most of the $V_{\rm oc}$ and FF results, which are relevant to the accuracy of the translation, are within $\pm 1\%$ throughout the irradiance range

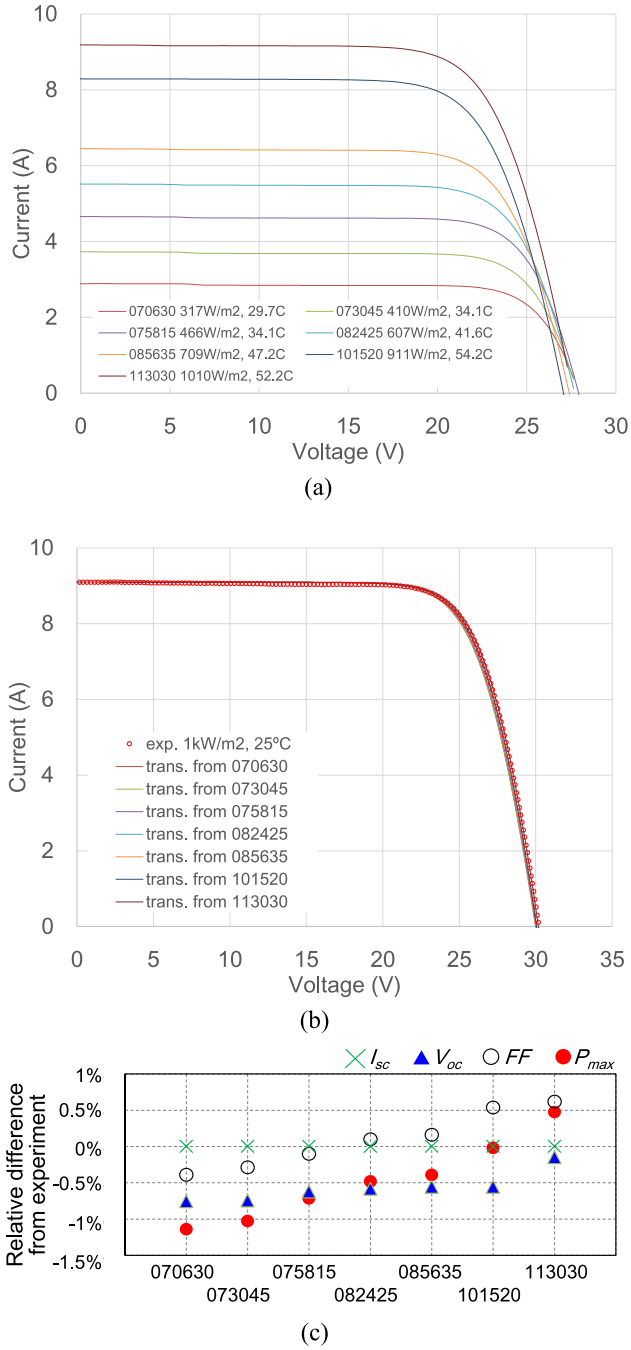

Fig. 5. (a) Outdoor *I–V* curves of N15B05. The measured irradiance and module temperature are indicated in the legend. (b) *I–V* curves translated to STC from the curves in (a). (c) Relative difference of the parameters of translated and experimental STC *I–V* curves as shown in (b).

of 0.3–1.05 kW/m^2, which are summarized in Table II with other MUTs' results. This indicates that those parameters of the translated *I–V* curves agree within $\pm 1\%$ of the indoor STC results. The deviation of $I_{\rm sc}$, shown by green symbols, is not because of the translation procedure in this result, since it is because of the irradiance measurement due to the slight difference in the installation angles and angular dependent optical reflectances between the MUT and PVMS [27], as well as, the small spectral mismatch between the MUT and PVMS [28], [29]. Possible

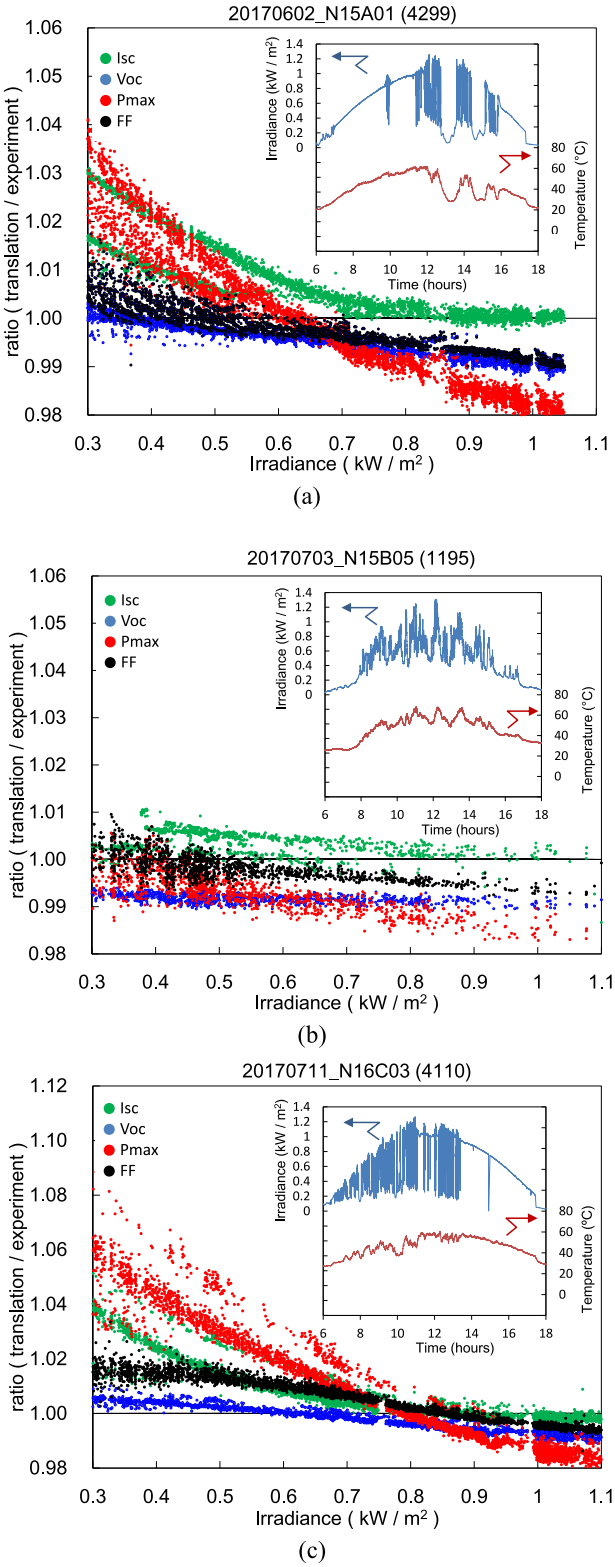

Fig. 6. Summary of the translation results for (a) N15A01, (b) N15B05, and (c) N16C03. The I_{sc}, V_{oc}, FF, and P_{max} values of the translated *I–V* curves relative to the indoor values are plotted by green, blue, black, and red symbols, respectively, versus the irradiance. The *I–V* curves measured at an interval of 5 s on one day for each module were translated by (5)–(8). The irradiance and module temperature are shown by the insets. The number of plotted data is indicated in the brackets at the top of each figure. The data are filtered for the R^2 of the plot in Fig. 2 and for the irradiance uniformity. Details of the conditions are described in the text.

TABLE II
PERCENTAGE OF DATA POINTS IN Fig. 6 WHICH FALL IN ±1% AND ±2% OF THE INDOOR STC RESULTS.

	V_{OC}		FF	
	±1%	±2%	±1%	±2%
N15A01 (Fig. 6(a))	96.8%	100.0%	99.0%	100.0%
N15B05 (Fig. 6(b))	97.2%	100.0%	100.0%	100.0%
N16C03 (Fig. 6(c))	99.5%	100.0%	72.9%	99.5%

nonlinearity of the MUT and PVMS also affects the deviation of I_{sc}. Data below 0.3 kW/m^2 are not shown, because the number of data in the linear part of the plot of Fig. 2 were often insufficient for determining R_s. Results for N15B05 in Fig. 6(b) show similar results, with better agreement in I_{sc}. N16C03 in Fig. 6(c) shows similar results, where most of the V_{oc} and FF results fall within ±2%, with larger deviation in I_{sc} and hence, in P_{max}. The agreement in I_{sc} is expected to be improved by accurately aligning the PVMS with the MUT, as well as, by using PVMSs which have similar angular dependence with the MUTs. Use of the same type of module as the MUT for PVMS will be an ideal choice for the latter purpose.

These results have demonstrated that the procedure of the present study based on (4)–(8) can translate indoor-measured and outdoor-measured *I–V* curves of crystalline silicon PV modules to STC without advance information of the translation parameters, and is applicable to wide irradiance and temperature ranges. The procedure is expected to be also applicable to PV devices other than crystalline silicon, such as III–V semiconductors and CIGS, as long as the devices follow the single-diode model (2), with the value nE_g/q modified according to the devices. The ±1%–2% deviation of the translated results from experiments in Figs. 4–6 can be caused by various factors, such as the estimation error of R_s, difference of nE_g/q from 1.232 V, and current mismatch among the component cells, as well as, the difference in the measured temperature of the modules' backsheet and that of their component cells [30]. Possible dependences of R_s and n [21] on the irradiance, temperature, voltage, and current also contribute to the results.

IV. CONCLUSION

The procedure of the present study has enabled accurate translation of the *I–V* curves of PV devices which follow the single-diode model (2) to other conditions such as STC, based on a single curve without advance information of the translation parameters. R_s used for the irradiance translation was extracted from the *I–V* curve by using a plot based on (4), and the TC was estimated by using a voltage-dependent formula (8) [5]. An *I–V* curve measured at any irradiance and temperature can be translated, as long as it follows the single-diode model (2), which can be judged by whether a straight plot based on (4) is available, as shown in Fig. 4(a) and (b). V_{oc} and FF of the *I–V* curves translated to STC from experimental curves measured at various irradiances (0.15–1.1 kW/m^2) and module temperatures (10–65 °C) showed good agreement typically within ±1%–2% with indoor experimental results.

REFERENCES

[1] *Photovoltaic Devices—Part 3: Measurement Principles for Terrestrial Photovoltaic (PV) Solar Devices With Reference Spectral Irradiance Data*, IEC 60904-3:2016, International Electrotechnical Commission, Geneva, Switzerland, 2016.

[2] *Photovoltaic Devices—Procedures for Temperature and Irradiance Corrections to Measured I–V Characteristics*, IEC 60891:2009, International Electrotechnical Commission, Geneva, Switzerland, 2009.

[3] Y. Tsuno, Y. Hishikawa, and K. Kurokawa, "Modeling of the *I–V* curves of the PV modules using linear interpolation/ extrapolation," *Sol. Energy Mater. Sol. Cells*, vol. 93, pp. 1070–1073, 2009.

[4] Y. Hishikawa, T. Takenouchi, M. Higa, and M. Yoshita, "New STC translation method for precise outdoor characterization of the *I-V* Curves of PV modules," (in Japanese), in *Proc. JSES/JWEA Joint Conf.*, Matsue, Japan, 2018, pp. 31–34.

[5] Y. Hishikawa *et al.*, "Voltage-dependent temperature coefficient of the *I–V* curves of crystalline silicon photovoltaic modules," *IEEE J. Photovolt.*, vol. 8, no. 1, pp. 48–53, Jan. 2018.

[6] Y. Hishikawa, T. Doi, M. Higa, K. Yamagoe, and H. Ohshima, "Precise outdoor PV module performance characterization under unstable irradiance," *IEEE J. Photovolt.*, vol. 6, no. 5, pp. 1221–1227, May 2016.

[7] Y. Hishikawa *et al.*, "Precise outdoor PV performance measurements at various irradiance levels," in *Proc. 43rd IEEE Photovolt. Spec. Conf.*, Portland, OR, USA, 2016, pp. 987–991.

[8] Y. Hishikawa *et al.*, "Effects of synchronous irradiance monitoring and correction of current–voltage curves on the outdoor performance measurements of photovoltaic modules," *Jpn. J. Appl. Phys.*, vol. 56, 2017, Art. no. 08MD07.

[9] D. Pysch, A. Mette, and S. W. Glunz, "A review and comparison of different methods to determine the series resistance of solar cells," *Sol. Energy Mater. Sol. Cells*, vol. 91, pp. 1698–1706, 2007.

[10] J. Montes-Romero *et al.*, "Comparative analysis of parameter extraction techniques for the electrical characterization of multi-junction CPV and m-Si technologies," *Sol. Energy*, vol. 160, pp. 275–288, 2018.

[11] G. M. M. W. Bissels *et al.*, "Theoretical review of series resistance determination methods for solar cells," *Sol. Energy Mater. Sol. Cells*, vol. 130, pp. 605–614, 2014.

[12] M. Wolf and H. Rauschenbach, "Series resistance effects on solar cell measurements," *Adv. Energy Convers.*, vol. 3, pp. 455–479, 1963.

[13] K. C. Fong, K. R. McIntosh, and A. W. Blakers, "Accurate series resistance measurement of solar cells," *Prog. Photovolt., Res. Appl.*, vol. 21, pp. 490–499, 2013.

[14] J. A. del Cueto, "Review of the field performance of one cadmium telluride module," *Prog. Photovolt., Res. Appl.*, vol. 6, pp. 433–446, 1998.

[15] M. Warashina and A. Ushirokawa, "Simple method for the determination of series resistance and maximum power of solar cell," *Jpn. J. Appl. Phys.*, vol. 19, no. 2, pp. 179–182, 1980.

[16] J. H. Werner, "Schottky barrier and pn-junction I/V plots—Small signal evaluation," *Appl. Phys. A*, vol. 47, pp. 291–300, 1988.

[17] M. K. El-Adawi and I. A. Al-Nuaim, "A method to determine the solar cell series resistance from a single *I–V*. Characteristic curve considering its shunt resistance—New approach," *Vacuum*, vol. 64, pp. 33–36, 2001.

[18] J. C. H. Phang, D. S. H. Chan, and J. R. Phillips, "Accurate analytical method for the extraction of solar cell model parameters," *Electron. Lett.*, vol. 20, pp. 406–408, 1984.

[19] V. N. Singh and R. P. Singh, "A method for the measurement of solar cell series resistance," *J. Phys. D, Appl. Phys.*, vol. 16, pp. 1823–1825, 1983.

[20] G. L. Araujo and E. Sanchez, "A new method for experimental determination of the series resistance of a solar cell," *IEEE Trans. Electron Devices*, vol. ED-29, no. 10, pp. 1511–1513, Oct. 1982.

[21] H. El Achouby, M. Zaimi, A. Ibral, and E. M. Assaid, "New analytical approach for modelling effects of temperature and irradiance on physical parameters of photovoltaic solar module," *Energy Convers. Manage.*, vol. 177, pp. 258–271, 2018.

[22] K. Ishibashi, Y. Kimura, and M. Niwano, "An extensively valid and stable method for derivation of all parameters of a solar cell from a single current–voltage characteristic," *J. Appl. Phys.*, vol. 103, 2008, Art. no. 094507.

[23] Y. Hishikawa *et al.*, "Temperature dependence of the short circuit current and spectral responsivity of various kinds of crystalline silicon photovoltaic devices," *Jpn. J. Appl. Phys.*, vol. 57, 2018, Art. no. 08RG17.

[24] *Photovoltaic Devices—Part 10: Methods of Linearity Measurement*, IEC 60904-10:2009, International Electrotechnical Commission, Geneva, Switzerland, 2009.

[25] J. Zhang, K. Watanabe, J. Yoshino, T. Kobayashi, Y. Hishikawa, and T. Doi, "Filtering method of detecting solar irradiance conditions for photovoltaic module performance characterization under unstable and nonuniform irradiance," *Jpn. J. Appl. Phys.*, vol. 57, 2018, Art. no. 08RG10.

[26] J. Zhang *et al.*, "Physical process and statistical properties of solar irradiance enhancement observed under clouds," *Jpn. J. Appl. Phys.*, vol. 57, 2018, Art. no. 08RG11.

[27] T. Doi *et al.*, "Analysis of angular dependence of PV module irradiance sensor using outdoor measured data—Intercomparison of various types of PVMSs and comparison between MUTs and PVMSs," (in Japanese), in *Proc. JSES/JWEA Joint Conf.*, Nagaoka, Japan, 2017, pp. 201–204.

[28] J. Chantana, H. Mano, Y. Horio, Y. Hishikawa, and T. Minemoto, "Spectral mismatch correction factor indicated by average photon energy for precise outdoor performance measurements of different type photovoltaic modules," *Renewable Energy*, vol. 114, pp. 567–573, 2017.

[29] Y. Horio, M. M. Rahman, Y. Imai, Y. Hishikawa, and T. Minemoto, "Impact of average photon-energy coefficient of solar spectrum on the short circuit current of photovoltaic modules," *Current Appl. Phys.*, vol. 17, pp. 1341–1346, 2017.

[30] K. Nishioka *et al.*, "Accurate measurement and estimation of solar cell temperature in photovoltaic module operating in real environmental conditions," *Jpn. J. Appl. Phys.*, vol. 57, 2018, Art. no. 08RG08.